

Chirped pulse amplification beam correction using computer generated holograms

L. IONEL*, C. P. CRISTESCU^a

National Institute for Laser, Plasma and Radiation Physics, Laser Department, Atomistilor Str. 409, P. O. Box MG-36, 077125 Magurele-Bucharest, Romania

^aDepartment of Physics I, Faculty of Applied Sciences, Politehnica University of Bucharest, 313 Splaiul Independentei, RO-060042, Bucharest, Romania

In this paper we present an alternative method to correct the shape of the Gaussian beam profile propagated through a chirped pulse amplification system employing computer generated holograms (CGHs). Considering the optical beam path from the experimental setup, we simulated the chirped pulse amplification Gaussian beam intensity profile using the numerical ray-tracing model from Rayica module of Mathematica. An iterative code based on Gerchberg-Saxton algorithm (GSA) was used to design computer generated holograms in order to make the correction of the aberrated Gaussian beam. The input images for GSA were generated in four distinct cases: after the stretcher and after the compressor using the dispersive element and in the same locations using an absorbent element. The results are relevant for different applications where the laser pulse shape correction is needed.

(Received August 2, 2011; accepted September 15, 2011)

Keywords: Chirped pulse amplification, Ray-tracing, Spatial light modulator, Computer generated hologram

1. Introduction

In the last decades, adaptive optical devices were successfully implemented in many applications such as: wave front correction [1], compensating time-varying aberration of optical fields [2], compensation thermal phase distortion occurring in high-energy glass amplifiers [3], beam steering, holographic optical tweezers [4], edge contrast improvement in light microscopy [5], holographic data storage, image processing and analysis [6]. Liquid crystal spatial light modulators (SLM) have been demonstrated recently as the most efficient reconfigurable opto-electronic element to compensate the aberrations of optical fields. These devices are able to modulate light spatially in amplitude and/or phase and the optical information to be displayed can be taken directly from the incorporated software or an image source and can be addressed directly by a computer interface. They can act like programmable phase masks [7], diffractive microlenses [8], multiple beam splitters [9], optical switches [10].

In this paper we combine two SLMs devices to create a dynamic and compact adaptive optical system in order to correct the beam profile resulted after propagation through a CPA (Chirped Pulse Amplification) laser system which contains two pulse shaping elements in the stretcher: an optical window and an absorbent element. The distortions of the CPA optical systems appear due to the different optical paths introduced in the stretcher at different wavelengths to create the group velocity dispersion which stretches the laser pulse to be amplified. Also, the distortions compensation in the compressor may not be perfectly achieved. Thus, we correct the aberrations of the

distorted Gaussian beam profile produced by two processes: the CPA main principle and the pulse shaping method.

The study is done in four cases: a dispersive element placed inside the CPA chain after the stretcher and after the compressor, respectively and an absorbent element placed in the same locations. All these intensity patterns were generated in Mathematica in accordance with the optical path from the chirped pulse amplification system, and were addressed on the first spatial light modulator. Starting with these images, we calculate CGHs using a MATLAB code based on Gerchberg-Saxton algorithm to correct the altered profiles. These CGHs are addressed on the second SLM. In this way we create a dynamic and compact adaptive optical system to correct the aberrated intensity distribution of the laser beam.

2. Ray-tracing simulation

Our experimental setup for chirped pulse amplification contains different components; the main ones are: an optical stretcher, an amplifier and a compressor for a laser system with 200 femtosecond pulses based on the CPA principle [11]. Starting from this arrangement, we design a compatible system using the ray-tracing model from Rayica module of Mathematica. As a final image, we obtain the distorted beam intensity profile to be corrected.

Fig. 1 shows a schematic of our optical stretcher-amplifier-compressor design. We used a diffraction grating with 1200 lines/mm and 110×110×16 mm dimensions. The spherical mirror with 6 inch diameter has the focal length of 1200 mm and it is placed about 780 mm

away from the diffraction grating and the roof top mirror ensures the double passing of the optical system. The incidence angle on the grating is 23° . The pulse duration after the stretcher is about 25 ps [12].

After the amplification, the output pulse is directed to the optical compressor, where it is recompressed back to the original pulse duration. The compressor includes two roof top mirrors, the vertical mobile roof top mirror to displace the beam for the two passes and one horizontal roof top mirror to fold the compressor. The total length of the stretcher and compressor, is about 14 m. The compressor uses the same incident angle as the stretcher.

This module uses a numerical ray-tracing model to extract the wavelength-dependent phase for each beam. The information relating to the profile intensity of the CPA Gaussian beam propagated through the simulated optical system is obtained after the optical stretcher and compressor. The distortion of the pulse is produced by positioning in front of the roof top mirror from the stretcher a dispersive and an absorbent element as can be seen in Fig. 1. These two pulse shaping elements are placed 40 mm away from the roof top mirror and their position is defined according to the center of the beam. In this way we obtained four intensity profiles of the distorted beam (see Fig. 2). In the second part of this work, we apply on the SLM the transmittance function $t_i(x,y)$, $i=1:4$, from Fig. 2, like a bidimensional (600×800 intercepted pixels) distribution of maximum 8-digit quantization of 256 gray levels in RGB mode. Each of them introduces a different value of the potential V_{rms} , which is electronically addressable on each pixel of the SLM.

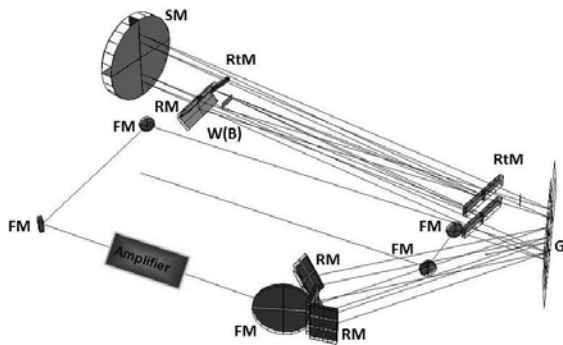


Fig. 1. Rayica ray-tracing of the stretcher-compressor system having only one diffraction grating G ; $W(B)$: dispersive (absorbent) element positioned in front of the roof top mirror in the optical stretcher; SM : spherical mirror; RM : roof top mirror; RtM : rectangular mirror; FM : flat mirror, after [12].

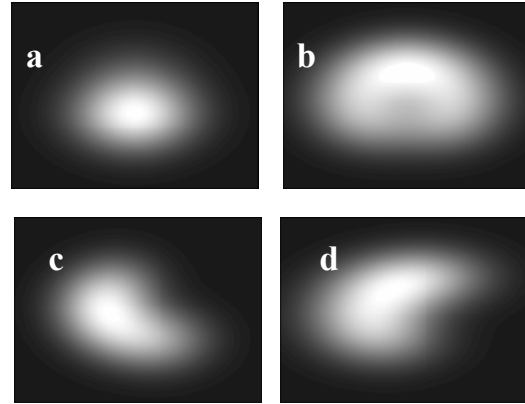


Fig. 2. The intensity profile of the aberrated beam according to the transmission function $t_i(x,y)$: a) $t_1(x,y)$ after the stretcher using the dispersive element; b) $t_2(x,y)$ after the compressor using a dispersive element; c) $t_3(x,y)$ after the stretcher using an absorbent element; d) $t_4(x,y)$ after the compressor using the absorbent element.

The dispersive element is a BK7 glass window, 10 mm wide and 5 mm thick which is placed in central position introducing a delay by its dispersion. The second optical element used to alter the Gaussian beam profile is an absorbent element with the same dimensions as the optical window shifted with 4 mm from the center of the beam. The optical baffle is generally used to produce a spectral clipping by obscuring completely a continuous part of the spectrum with variable bandwidth, the “blue” one (short wavelengths) or the “red” one (long wavelengths) [13]. In our case, the clipped part of the spectrum is the red one from 778 nm up as it can be seen in Fig. 3.

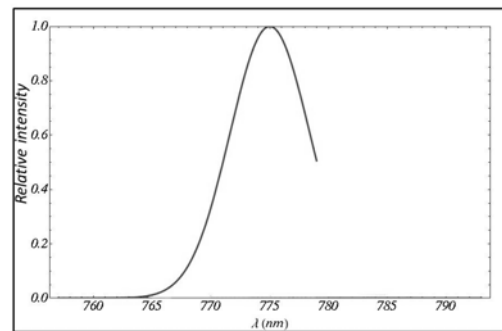


Fig. 3. Spectrum of the clipped pulse produced by the absorbent element above 778 nm wavelength.

Beside the effect introduced by these two pulse shaping elements, the distortion of the pulse also appears during the group velocity dispersion process in the CPA system. This is possible by introducing different optical paths at different wavelengths in the lasing range which produces a spatial chirp at the roof top mirror in the stretcher. This geometrical property can be compensated by the second pass through the stretcher. The spectral

chirp is accumulated with each pass and determines the group delay dispersion.

In order to compensate the aberrations introduced in our system by the CPA method, we use the Gerchberg-Saxton algorithm [14] which is able to retrieve the phase function across a wave front. The algorithm is adapted in order to fulfill the constrains for our components and it is used to obtain the computer generated hologram for each of the four cases, containing: the amplitude and the phase, the amplitude-only and the phase-only of the desired image. This algorithm is applied in both holograms (SLM) and object image reconstruction planes.

3. Diffractive pattern for the second SLM design

A suitable scheme [15] of the GSA, implemented in MATLAB, was employed to calculate the diffractive pattern which is addressed on the second SLM. It simulates the backward and forward propagations between the input plane (CGH plane considered in the second SLM plane) and the output plane (image plane considered in the screen plane). The input variables are:

1. incident illumination
 - the four images from Fig. 2
2. desired pattern in the image plane
 - a Gaussian intensity profile
3. initial phase in the image plane
 - constant
4. the number of the phase levels in the CGH plane
 - eight for our SLM

The output image is the phase distribution in CGH plane which is addressed on the second SLM.

The images generated in Rayica are sampled taking into account the Nyquist criterion [16] and they become discrete transmission function which correspond with the experimental intensity distribution in the CPA system. The discrete coordinates are:

$$x = m \cdot \Delta p, \quad y = n \cdot \Delta p,$$

$$x_z = m_z \cdot \Delta p_z, \quad y_z = n_z \cdot \Delta p_z,$$

where n and m are the numbers of the pixels in x and y directions, Δp and Δp_z , are the pixels dimensions in the CGH plane and in the image plane respectively. These images are considered for incident illumination in GSA.

Our study investigates also the numerical possibilities to have a complex incident wavefront. This complex plane wave (with amplitude $A(x,y)$ and normalized phase $\varphi(x,y)$):

$$C(x,y) = A(x,y) \cdot \exp[i \pi \varphi(x,y)]$$

incident on the second SLM was generated in three different cases:

$$\alpha) A(x,y) = t_i(x,y) \text{ and } \varphi(x,y) = t_i(x,y);$$

$$\beta) A(x,y) = t_i(x,y) \text{ and } \varphi(x,y) = \pi;$$

$$\gamma) A(x,y) = 1 \text{ and } \varphi(x,y) = t_i(x,y).$$

$$i=1:4$$

According to these considerations we generated the computer holograms for all four cases. In Fig. 4 the cases $\alpha \rightarrow \gamma$ are presented only for the case when the pattern generated in Rayica is considered as incident illumination after the stretcher using the dispersive element as shown in Fig. 2a. In Fig. 4 are presented fragments from CGHs computed in cases $\alpha \rightarrow \gamma$ which have 600×800 pixels.

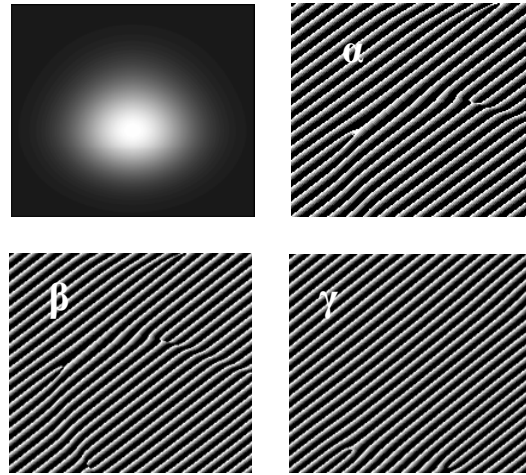


Fig. 4. Computer generated hologram using IFTA algorithm obtained after the stretcher using the dispersive element, containing: α) the amplitude and the phase; β) the amplitude-only and γ) the phase-only of the desired image.

Before we apply the GSA algorithm, the initial phase in the image plane is maintained constant. After the algorithm is run in order to design the computer generated holograms from the desired image, this process is iterated till the best diffraction efficiency is obtain.

The constraint which is put on the final matrix to be transferred on the second SLM is to maintain the amplitude constant ($A(x,y)=1$) and the final phase is discretized to take maximum eight grey levels due to the SLM fabrication restraints.

4. Experimental results

A sketch of the experimental setup is shown in Fig. 5. We used as light source a laser diode with an emission spectrum centered in 650 nm followed by a telescope to enlarge the laser spot and ensure a proper illumination of all active area of the first SLM. Two computers were used to address the aberrated intensity profile on the first SLM (the four cases Fig. 2) and the corresponding CGH on the second SLM. The optical system composed by these two SLMs is fitted by two linear sheet polarizers.

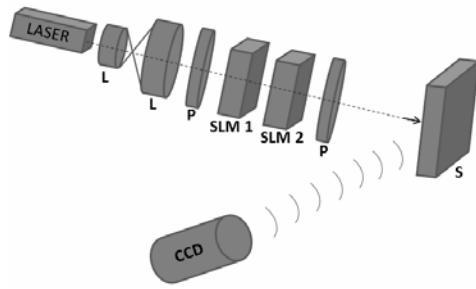


Fig. 5. The experimental setup for the CPA beam intensity profile correction. L: lens; P: polarizer; S: diffraction plane.

We address on the first SLM used in the experiment the images obtained in Mathematica with aberrated intensity profiles presented in Fig. 2. The output intensity distribution obtained from it represents the incident illumination on the second SLM (like in simulation for CGH design). In our four cases, the images are presented in Fig. 6. The distance between the first and the second SLM is 0.5 mm. The second SLM creates in far field the corrected Gaussian beam profile.

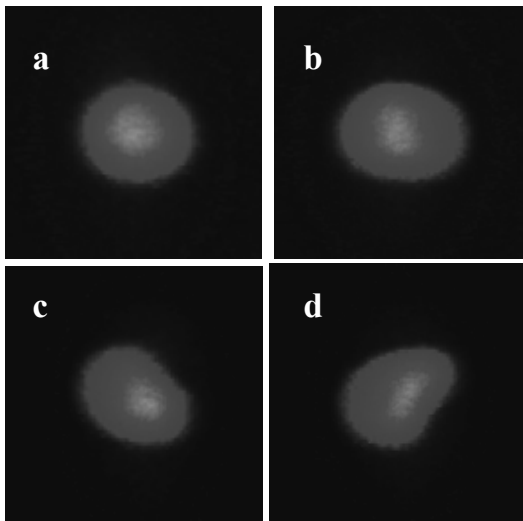


Fig. 6. The output intensity distribution from the first SLM corresponding to the aberrated Gaussian beam obtained: a) after the stretcher using the dispersive element; b) after the compressor using a dispersive element; c) after the stretcher using an absorbent element; d) after the compressor using the absorbent element.

The SLMs are identical twisted nematic liquid crystals displays from Sony Model LCX016AL, with $26,6 \times 20$ mm active area, with a VGA graphic card resolution (800 columns and 600 rows active pixels), $32 \mu\text{m}$ pitch, 200:1 contrast ratio, 60 Hz image frame rate, nearly phase-only modulation, acceptable response time (~ 5 ms), increased fill factor.

The final images (after the second SLM) are recorded on the CCD (Pike F421C resolution 2048×2048 , $7.4 \mu\text{m}$

pixel pitch, 75 fps) which was placed at distance of 1 meter from the second SLM plane.

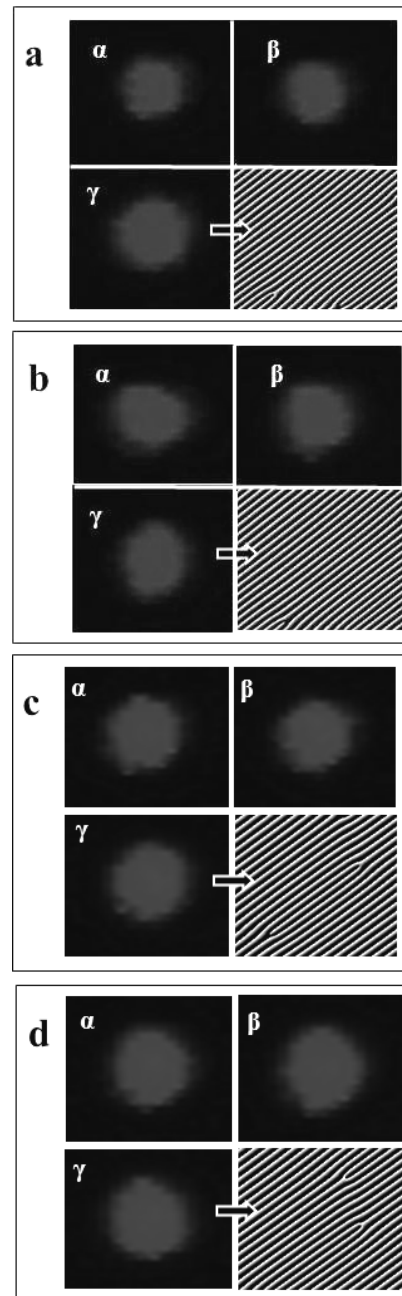


Fig. 7. Correction of the beam shape resulted after the CPA system when the associate phase-only map is addressed on the SLMs in four cases: a) stretcher using a dispersive element; b) compressor using a dispersive element; c) stretcher using an absorbent element; d) compressor using an absorbent element. The diffraction patterns $\alpha \rightarrow \gamma$ corresponds to the cases from Fig. 4. A filter is added in front of the CCD to avoid its sensor saturation.

The relation between the dimensions of the pixel in the output plane and the dimensions of the pixel in the SLM plane is given in reference [17]:

$N\Delta x\Delta x_1 = \lambda d$, and $M\Delta y\Delta y_1 = \lambda d$, where N and M are the numbers of the pixels in x and y directions, Δx , Δy and Δx_1 , Δy_1 represents the dimensions of one pixel in the input and output plane, respectively on both axes d is the distance between them.

A typical result is presented in Fig. 7a and b for the case considered in Rayica with a glass window after the stretcher and compressor. There are shown the diffraction patterns obtained after we applied on the second SLM the computer generated holograms using GSA algorithm. The three cases represent the numerical investigations for incident illumination: α) amplitude and phase, β) amplitude-only and γ) phase-only. The computer generated holograms illustrated in these two cases contain information in phase-only discretized on eight levels and they provide the best correction of the aberrated intensity profile to the Gaussian beam.

In a similar way, Figs. 7c and d show the results obtained with Rayica for the case with absorbent after the stretcher and compressor. The best adjustment for the shape of the aberrated Gaussian beam in both cases is made when we address to the second SLM the CGH designed using in GSA the incident illumination only with phase information and constant amplitude.

5. Conclusions and discussion

We present a dynamic and fast method for the aberrated beam intensity profile correction using two spatial light modulators.

The aberrated beams result in the experimental setup based on CPA method generally used to provide higher intensity in laser systems. This setup is modeled numerically in Rayica and four cases are investigated after the stretcher and after compressor when we use two pulse shaping elements introduced in the stretcher. The final images in these cases are considered further for correction.

To correct the aberrated beam, we employ GSA to calculate the CGH in the four cases (a→d) listed above. In GSA, the four images from Rayica are considered like initial illumination. We investigate numerically the cases for different incident complex waves (in amplitude and phase). When the desired output image is a Gaussian one.

To verify experimentally our numerical procedure, we built a setup with two SLMs. On the first we address the images from Rayica and on the second we address the holograms generated in three cases (α → γ) mentioned above for amplitude and phase. The CGHs generated with phase-only incident illumination (γ) give the best results in the four cases considered (a→d). Thus, the shape of the laser spot obtained in the diffraction pattern is more circular than the other two cases (α and β).

We demonstrated that this combination for shape of the intensity profile correction is possible using CGHs addressed on the SLM computed with a given incident illumination. The advantage of this alternative method of Gaussian beam correction is that it can be used for laser

systems with fluence threshold of 50 mJ/cm² in continuous mode which is equivalent to 2 W power in pulsed regime. This method will be easily implemented on our CPA laser system output in order to compensate the distortions of the pulse during the propagation through the laser system and to improve the quality of the laser beam profile used for different applications.

References

- [1] A. Jesacher, A. Schwaighofer, S. Fürhapter, C. Maurer, S. Bernet, M. Ritsch-Marte, *Optics Express*, **15**(9), 5803 (2007).
- [2] J. W. Hardy, *Adaptive Optics for Astronomical Telescopes*, Oxford University Press, New York (1998).
- [3] B. Wattellier, J. C. Chanteloup, J. Fuchs, C. Sauteret, J. P. Zou, A. Migus, in *Conference on Lasers and Electro-Optics*, Vol. **56** of OSA Trends in Optics and Photonics Series, Optical Society of America, Washington, D.C., 70 (2001).
- [4] E. R. Dufresne, D. G. Grier, *Rev. Sci. Instrum.* **69**, 1974 (1998).
- [5] S. Fürhapter, A. Jesacher, S. Bernet, M. Ritsch-Marte, *Opt. Express* **13**, 689 (2005).
- [6] A. I. Nagaev, V. N. Parygin, S. Iu. Pashin, *Soviet Journal of Quantum Electronics*, **12**, 1178 (1982).
- [7] A. M. Weiner, *Rev. Sci. Instrum.* **71**, 1929 (2000).
- [8] M. Mihailescu, A. M. Preda, A. Sobetkii, A. C. Petcu, *Opto-Electronics Review*, Springer **17**(4), 330 (2009).
- [9] A. Moradi, E. Ferrari, V. Garbin, E. Fabrizio, D. Cojoc, *Optoelectron. Adv. Mater.- Rapid Commun.* **1**(4), 158 (2007).
- [10] S. Aherom, M. Raisi, K. Lo, K. E. Alameh, R. Mavaddat, *High Speed Networks and Multimedia Communications 5th IEEE International Conference*, 239 (2002).
- [11] L. Ionel, C. P. Cristescu, F. Jipa, M. Enculescu, M. Radoiu, R. Dabu, M. Zamfirescu, M. Ulmeanu, *Optoelectron. Adv. Mater. - Rapid Commun.* **4**(11), 1920 (2010).
- [12] D. Ursescu, L. Ionel, *J. Optoelectron. Adv. Mater.* **12**(1), 48 (2010).
- [13] D. Ursescu, L. Ionel, C. P. Cristescu, *U. P. B. Sci. Bull., A*, **70**(4), 49 (2008).
- [14] R. W. Gerchberg, W. O. Saxton, *OPTIK*, **35**(2), 237 (1972).
- [15] M. Mihailsescu, A. Preda, D. Cojoc, E. Scarlat, L. Preda, *J. Optoelectron. Adv. Mater.* **9**(4), 1071 (2007).
- [16] M. Mihailescu, A. M. Preda, A. Sobetkii, E. Scarlat, L. Preda, *U.P.B. Sci. Bull., Series A*, **69**(3), 25 (2007).
- [17] J. García, D. Mas, R. G. Dorsch, *Appl. Opt.* **35**(35), 7013 (1996).

*Corresponding author: laura.ionel@infpr.ro